ICAS 2021 SHANG HAI
International Council of the Aeronautical Sciences
32nd Congress of the International Council of the Aeronautical Sciences
September 6-10, 2021
Pudong Shangri-La, Shanghai, China

AERODYNAMIC OPTIMIZATION DESIGN OF DOUBLE BLUNT ROTOR AIRFOIL WITH LARGE THICKNESS IN FORWARD AND REVERSE FLOW

YiMing YAO[1], XuDong YANG[1]

[1]School of Aeronautics, Northwestern Polytechnical University, Xi'an, China

Abstract

The double blunt rotor airfoil located at the root segment of the coaxial rigid rotor helicopter blades has been proved to be effective in suppressing the flow separation of retreating blades in reverse flow, so as to effectively reduce the drag coefficient and improve the flight efficiency. However, the complicated flow field environment caused by counter-rotating blades and various flight states of the coaxial rigid rotor helicopter put forward more design points and higher performance requirements for the double blunt rotor airfoil. In this paper, a multi-objective aerodynamic optimization method with complex constraints based on Kriging models and hypervolume is developed to optimize the double blunt rotor airfoils with a relative thickness of 26% and 40% respectively in forward and reverse flow. After the optimization, the full turbulence and free transition calculation based on Reynolds Averaged Navier-Stokes (RANS) equations for the airfoils before and after the optimization are conducted, the results show that the optimized rotor airfoils generally meet the design indicators proposed in this paper with all constraints being satisfied, the drag coefficients in a wide range of Mach numbers are reduced, and the vibration of the optimized airfoils is alleviated to a certain extent in reverse flow.

Keywords: multi-objective optimization, airfoil shape optimization, Kriging model, hypervolume, computational fluid dynamics

1. General Introduction

Coaxial rigid rotor helicopters based on the Advancing Blade Concept (ABC), which have excellent high-speed forward flight performance and good maneuverability, have gradually become the development trend of high-speed helicopters [1][2]. To solve the problem that the root segment of the retreating blades is left in the reverse flow when flying forward at high speed, Sikorsky applied a 'double blunt' airfoil (DBLN526) with a relative thickness of 26% at the root segment of the X2TD coaxial rigid rotor verification aircraft. It was verified by experiments that this kind of airfoil can effectively suppress the reverse flow at the root segment of the retreating blades, suppress the separation of the airflow, reduce the drag and noise, and greatly improve the high-speed forward flight efficiency [3].

However, compared with the conventional single rotor, the flow field environment of the coaxial rigid rotor is more special. Due to the mutual influence of the upper and lower rotor, the unsteady characteristics of the flow field are more complicated. The retreating blades are in special operating environments such as reverse flow in a large area, periodic changes in the angle of attack of the inflow, and dynamic stalling, which require the airfoil at the root segment of the blade to maintain a low drag coefficient and reduce the vibration when the forward and reverse flow alternates. On the other hand, the forward flight, hovering, maneuvering and other flight states of the coaxial rigid rotor helicopters put forward more design points and higher performance requirements for the rotor airfoil. For example, wider range of working Mach numbers, small pitching moment coefficient, excellent dynamic characteristics, etc. Therefore, the design of double blunt rotor airfoil is a multi-objective and multi-constraint aerodynamic shape optimization design problem under multiple design points.

In the multi-objective and multi-constraint aerodynamic shape optimization problems, the design objectives are usually in conflict with each other. Multi-objective evolutionary algorithm (MOEA) can obtain a Pareto front (PF) with good distribution and convergence for decision makers. However, the disadvantage of this method is that it requires real function evaluations on a large number of sample points in each iteration, which is extremely expensive. The multi-objective aerodynamic shape optimization method based on surrogate model can effectively reduce the number of computational fluid dynamics (CFD) analysis and significantly improve the efficiency of optimization, which is a research hotspot in the field of aerodynamic shape optimization. The commonly used surrogate models include Kriging, polynomial response surface models (PRSM), radial-basis functions (RBFs), artificial neural network (ANN), etc. Kriging model has a good capability in fitting high-dimensional and nonlinear functions [4], which can not only predict the value of an unknown location, but also provide the error estimation at the same time, so it is widely used in aerodynamic shape optimization and design [5].

The early Kriging-based method only took the prediction value of Kriging model as the fitness value of multi-objective evolutionary algorithm to optimize, which depends on the accuracy of the Kriging model, and the efficiency decreases sharply with the increase of the number of design variables [6][7][8]. Afterwards, efficient global optimization (EGO) method proposed by Jones [9] was introduced and successfully extended in multi-objective aerodynamic shape optimization problems. For example, Kanazaki [10] and Obayashi [11] obtained the PF of the expected improvement (EI) functions corresponding to the objective functions by using a multi-objective genetic algorithm, and then selected the intermediate and boundary sample points to update the Kriging model, the proposed method was applied in a multi-segment airfoil multi-objective optimization problem. Keane [7] proposed a multi-objective EI criterion (multi-EI), all of the sample points of the current PF were selected as new sample points. However, the multi-objective optimization methods based on Kriging models mentioned above do not consider the quality of multi-objective optimization solution set, the optimization is not efficient and it is difficult to get the expected Pareto solution set. To solve this problem, indictor-based multi-objective optimization methods were proposed. Among the proposed quality indicators, hypervolume (HV) [12] was widely studied and applied in real-world multi-objective optimization problems because it considers both the convergence and diversity of the solution set. For example, Beume [13] proposed SMS-EMOA based on HV and non-dominated sorting method and applied it to airfoil aerodynamic shape optimization problems, the results showed that the optimization efficiency of the method was significantly improved. Emmerich [14] et al. proposed expected hypervolume improvement (EHVI) infill sampling criterion. Shimoyama [15] et al. compared the performance of EHVI and EI in bi-objective optimization problems and found that EHVI was more efficient than EI in unconstrained problems. Jesús Martínez-Frutos [16] et al. implemented constraint handling for EHVI. Zuhal [17] implemented EHVI in three airfoil multi-objective optimization problems and found that EHIV performed the best compared with ParEGO [18] and Euclidean-based expected improvement (EEI). As a potential method in multi-objective aerodynamic optimization, EHVI was suggested to be further explored and studied.

This paper aims to reduce the drag coefficient of the double blunt rotor airfoil at the root segment of the blades in forward and reverse flow, and optimizes the double blunt airfoil DBLN526 with a relative thickness of 26% to further improve its performance, in order to obtain the airfoil with better structural performance, the double blunt airfoil with a relative thickness of 40% is also optimized. In the optimization process, this paper establishes a multi-objective aerodynamic optimization design method based on Kriging models, and uses an infill-sampling strategy based on hypervolume in the sub-optimization. The airfoils before and after optimization are evaluated by the full turbulence and free transition calculation based on Reynolds Averaged Navier-Stokes (RANS) equations.

2. Multi Objective Optimization Method Based on Kriging Model and Hypervolume

2.1 Kriging Predictor and Mean Squared Error

Kriging model takes the unknown function as the concrete realization of a static stochastic process, which can be defined as follows [9]:

$$Y(\mathbf{x}) = \beta_0 + Z(\mathbf{x}) \tag{1}$$

where $\mathbf{x}$ is the vector of m-dimensional design variables and $Y(\mathbf{x})$ is the unknown function of interest, the trend function β_0 is an unknown constant, which represents the mathematical expectation of $Y(\mathbf{x})$, and $Z(\mathbf{x})$ is a stochastic process with zero mean and a covariance of

$$Cov\left[Z(\mathbf{x}), Z(\mathbf{x}')\right] = \sigma^2 R(\mathbf{x}, \mathbf{x}') \tag{2}$$

where σ^2 is the process variance of $Z(\mathbf{x})$, $R(\mathbf{x}, \mathbf{x}')$ is the spatial correlation function which only depends on the Euclidean distance between the sample points $\mathbf{x}$ and $\mathbf{x}'$.
Assuming the prediction of the unknown function can be approximated by a linear combination of the observed data $\mathbf{y_s}$, the kriging predictor of $y(\mathbf{x})$ at an unknown point $\mathbf{x}$ can be expressed as follows:

$$\hat{y}(\mathbf{x}) = \mathbf{w}^{\mathbf{T}} \mathbf{y_s} \tag{3}$$

where $\mathbf{w} = \left[w^{(1)}, w^{(2)} \cdots, w^{(n)}\right]^T$ is the vector of weight coefficients. Under the condition of unbiased estimation, the mean square error (MSE), which is defined as follows, is minimized.

$$MSE[\hat{y}(\mathbf{x})] = E\left[\left(\hat{y}(\mathbf{x}) - Y(\mathbf{x})\right)^2\right] \tag{4}$$

Then the predicted value of the Kriging model at any unknown point $\mathbf{x}$ is:

$$\begin{gathered} \hat{y}(\mathbf{x}) = \beta_0 + \mathbf{r}^{\mathrm{T}}(\mathbf{x}) \mathbf{R}^{-1}\left(\mathbf{y}_{\mathrm{S}} - \beta_0 \mathbf{F}\right) \\ \text{where} \quad \beta_0 = \left(\mathbf{F}^{\mathrm{T}} \mathbf{R}^{-1} \mathbf{F}\right)^{-1} \mathbf{F}^{\mathrm{T}} \mathbf{R}^{-1} \mathbf{y}_{\mathrm{S}},\ \mathbf{F} = [1, \ldots, 1]^T \\ \mathbf{R} = \left(R\left(\mathbf{x}^{(i)}, \mathbf{x}^{(j)}\right)\right)_{i,j} \in \mathbb{R}^{n \times n},\ \mathbf{r} = \left(R\left(\mathbf{x}^{(i)}, \mathbf{x}\right)\right)_i \in \mathbb{R}^n \end{gathered} \tag{5}$$

The mean square error of the Kriging prediction is:

$$\mathrm{MSE}\left\{\hat{y}(\mathbf{x})\right\} = s^2(\mathbf{x}) = \sigma^2 \left\{1.0 - \mathbf{r}^{\mathrm{T}} \mathbf{R}^{-1} \mathbf{r} + \left(1 - \mathbf{F}^{\mathrm{T}} \mathbf{R}^{-1} \mathbf{r}\right)^2 / \mathbf{F}^{\mathrm{T}} \mathbf{R}^{-1} \mathbf{F}\right\} \tag{6}$$

2.2 Infill Sampling Criteria Based on Hypervolume

As mentioned in the introduction, in the multi-objective aerodynamic optimization based on surrogate models, infill sampling criterion based on hypervolume is considered to be a potential method suggested to be further explored and studied. Here we introduce the two criteria used in this paper. The first one is called Constrained Maximization of Hypervolume Prediction (CMHVP), in which the sample point with the highest quality of Pareto solution set is directly found, while in the second criterion called Constrained Expected Hypervolume Improvement (CEHVI), the quantity and the probability of the improvement in the quality of solution set are both considered. Therefore, the combination of the two criteria will have higher global exploration efficiency with better local exploitation ability.

2.2.1 Constrained Maximization of Hypervolume Prediction (CMHVP)

The hypervolume (HV) of the non-dominated solution set is defined as follows [16]:

$$HV\left(\mathbf{PF},\mathbf{f}_{ref}\right)=Lebesgue\left(\left\{\mathbf{f}\in\mathbb{R}^{n}|\ \mathbf{PF}\preceq\mathbf{f}\preceq\mathbf{f}_{ref}\right\}\right) \tag{7}$$

where $\mathbf{PF}$ is the front of non-dominated solutions, $\mathbf{f}_{ref}$ is the reference point, $\mathbf{f}$ is the feasible solutions and $Lebesgue$ represents the Lebesgue measure.

The first infill sampling criterion called CMHVP used in this paper directly searches the location $\mathbf{x}_{add}$ with the maximum value of hypervolume on the Kriging models. For multi-constraint optimization problems, Kriging models are built for each constraint function $G_i\left(\mathbf{x}\right)\le 0$ and assume a random variable $G_i\left(\mathbf{x}\right)\sim N\left(\hat{g}_i\left(\mathbf{x}\right),\hat{s}^2_{g,i}\left(\mathbf{x}\right)\right)$, thus the constrained hypervolume prediction (CHVP) can be calculated by multiplying each probability that satisfies the constraint:

$$CHVP=\begin{cases}HV\left(\mathbf{PF}\cup\hat{\mathbf{f}},\mathbf{f}_{ref}\right)\cdot\prod_{i=1}^{N_G}\Phi\left(-\dfrac{\hat{g}_i(\mathbf{x})}{s_{g,i}(\mathbf{x})}\right) & \text{if } \hat{\mathbf{f}}\preceq\mathbf{PF}\\ HV\left(\mathbf{PF},\mathbf{f}_{ref}\right) & \text{otherwise}\end{cases} \tag{8}$$

where $\hat{\mathbf{f}}$ is the Kriging prediction at point $\mathbf{x}$ and N_G is the number of constraints. By optimizing the learning function above, the optimal solution with the largest CMHVP is found.

2.2.2 Constrained Expected Hypervolume Improvement (CEHVI)

EHVI is the expected value of hypervolume improvement (HVI) after the additional point $\mathbf{x}_{add}$ is added. It can be calculated as follows [16]:

$$EHVI=\int \mathrm{HVI}\left(\mathbf{PF},\hat{\mathbf{f}}\left(\mathbf{x}_{add}\right),\mathbf{f}_{ref}\right)\bullet pdf\left(\hat{\mathbf{f}}\right)d\hat{\mathbf{f}} \tag{9}$$

where $\hat{\mathbf{f}}\left(\mathbf{x}_{add}\right)$ is the Kriging prediction at point $\mathbf{x}_{add}$, $pdf\left(\hat{\mathbf{f}}\right)$ is the multidimensional probability density function of the objective functions.

The second infill sampling criterion called CEHVI used in this paper focuses on the improvement of PF in the whole multi-objective design space. Similar to the constraint handling method used in CMHVP, the learning function can be defined as follows:

$$Maximize: CEHVI=\prod_{i=1}^{N_G}\Phi\left(-\frac{\hat{g}_i\left(\mathbf{x}\right)}{s_{g,i}\left(\mathbf{x}\right)}\right)\cdot\int \mathrm{HVI}\left(\mathbf{PF},\hat{\mathbf{f}}\left(\mathbf{x}_{add}\right),\mathbf{f}_{ref}\right)\bullet pdf\left(\hat{\mathbf{f}}\right)d\hat{\mathbf{f}} \tag{10}$$

2.3 Algorithm Framework

This paper extends the EGO method proposed by Jones [9] to a multi-objective form by implementing CMHVP and CEHVI infilling strategy. Firstly, based on the baseline airfoil, a design of experiments (DoE) method, which is Latin Hypercube Sampling (LHS) in this paper, is used to generate a certain number of initial sample points. Secondly, by running high-fidelity simulations (CFD solver), the functional responses corresponding to the initial sample points are obtained. Thirdly, Kriging models are built for all objective functions and the constraint functions and trained based on the sample data. After that, the sub-optimization problems defined by CMHVP and CEHVI are solved to obtain two new candidate sample points. Finally, the sample points are evaluated by high-fidelity simulations again and augmented to the sample database to rebuild the Kriging models. The updating process is repeated until the convergence condition is satisfied. In the surrogate-based optimization (SBO) [19] module, Genetic Algorithm (GA) and BFGS optimization algorithm are used to find the optimal solutions of the learning functions defined by CMHVP and CEHVI. The flow chart of the algorithm framework is shown in Figure 1.

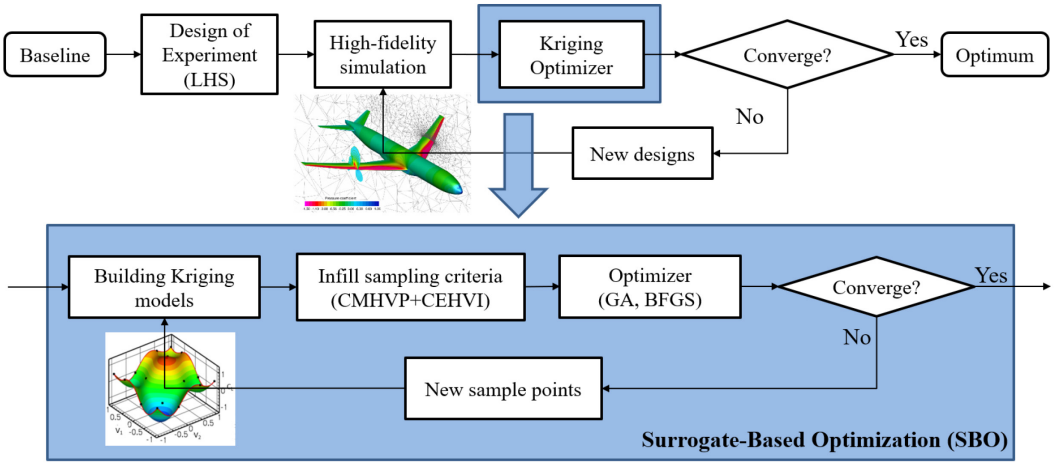

Figure 1 – Flowchart of multi-objective aerodynamic optimization design method based on Kriging models and hypervolume.

3. Double Blunt Rotor Airfoil Optimization

3.1 Problem Definition

In this sub-section, the design objectives and constraints are given by analyzing the flow field environment of the double blunt rotor airfoil. Take DBLN526 airfoil with a relative thickness of 26% as an example, according to the velocity distribution along the spanwise direction of the advancing and retreating blades of a coaxial rigid rotor helicopter during forward flight and hovering, the minimum and the maximum Mach number is about 0.2 and 0.5 respectively in forward flow, while in reverse flow, the maximum Mach number is about 0.22. Therefore, this paper focuses on the reduction of the drag coefficient at the conditions of medium angles of attack between Mach 0.3 to 0.5 in forward flow, on the other hand, the reduction of the drag coefficient at Mach 0.2 in reverse flow is also taken into consideration. The baseline airfoil with a relative thickness of 26% is DBLN526, while the baseline airfoil with a relative thickness of 40% is NWPU-CR-4000, which is obtained by changing the thickness of DBLN526. The design points, objectives and constraints of the two airfoil shape optimization problems are shown in Table 1. The superscript of the aerodynamic coefficient symbol represents the number of design points, and the dash above the symbol represents the average value of the aerodynamic coefficients at positive and negative angle of attack. The triangle symbol in the constraint column represents the change of the parameter of the airfoil before and after optimization. w_i is the weight coefficient of each design point, in this paper, w_i is set as $w_1=w_4=0.18$, $w_2=w_5=0.32$, $w_3=w_6=0.5$.

Table 1 – Objectives and constrains for airfoil shape optimization problems

Baseline	Objectives	Design points	Constraints
DBLN526	$\min.\ \bar{C}_d^1$ $\min.\ \sum_{i=2}^{4} w_i \bar{C}_d^i$	1.Ma=0.2, Re=1.4×10^6, α=±2°(reverse) 2.Ma=0.3, Re=2.2×10^6, α=±6° 3.Ma=0.4, Re=2.9×10^6, α=±4° 4.Ma=0.5, Re=3.6×10^6, α=±2°	$g_1=\Delta\lvert\sum_{i=2}^{4} w_i \bar{C}_m^i\rvert \le 0.005$ $g_2=\Delta(T/c)\ge 0$ $g_3=\Delta Area \ge 0$
NWPU-CR-4000	$\min.\ \sum_{i=1}^{3} w_i \bar{C}_d^i$ $\min.\ \sum_{i=4}^{6} w_i \bar{C}_d^i$	1.Ma=0.3, Re=2.2×10^6, α=±10°(reverse) 2.Ma=0.4, Re=2.9×10^6, α=±6°(reverse) 3.Ma=0.5, Re=3.6×10^6, α=±2°(reverse) 4.Ma=0.3, Re=2.2×10^6, α=±10° 5.Ma=0.4, Re=2.9×10^6, α=±6° 6.Ma=0.5, Re=3.6×10^6, α=±2°	$g_1=\Delta\lvert 0.5\sum_{i=1}^{3} w_i \bar{C}_m^i +$ $0.5\sum_{i=4}^{6} w_i \bar{C}_m^i\rvert \le 0.005$ $g_2=\Delta(T/c)\ge 0$ $g_3=\Delta Area \ge 0$

As shown in Table 1, the two optimization problems are both aimed at reducing the drag coefficient in forward flow and reverse flow respectively. At the same time, in order to maintain good maneuverability of the airfoil, the pitching moment coefficient is required to be constrained, and the relative thickness and area are not less than that of the baseline airfoil. The airfoil geometry is parameterized by a fifth-order CST method [20], and the sample points are evaluated by XFoil [21].

3.2 Results and Discussion

3.2.1 Aerodynamic Performance Using Full Turbulence Calculation

In the optimization of airfoils with relative thicknesses of 26% and 40%, one sample point with the best comprehensive performance in the Pareto front is selected as the final optimal airfoil to be evaluated and analyzed in detail. The shape comparison of the new airfoils with baselines is shown in Figure 2.

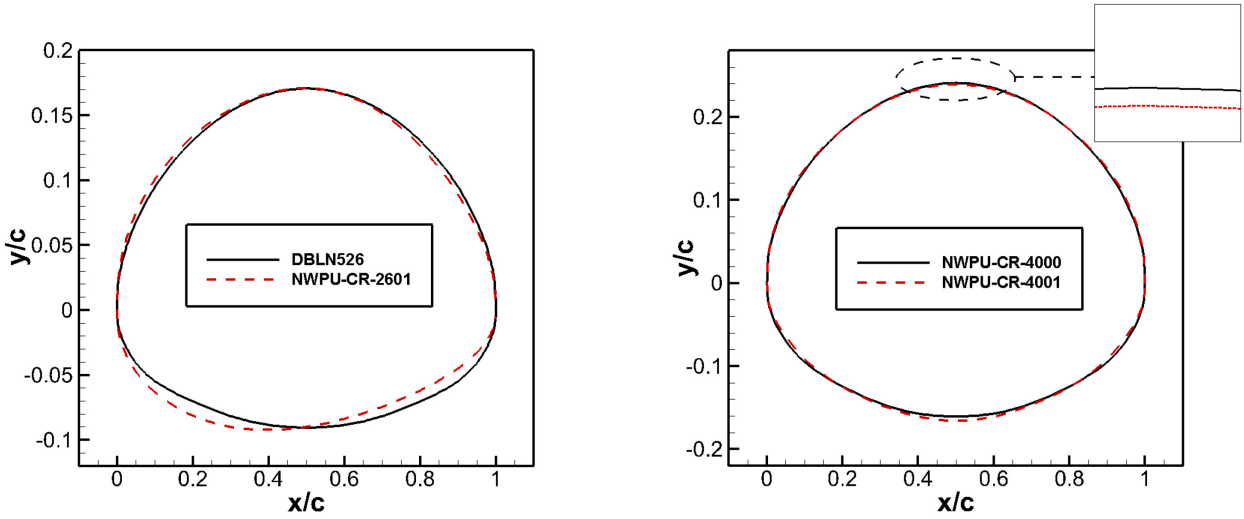

Figure 2 – Shape comparison between baseline and optimized airfoil.

In this sub-section, the baseline airfoil and the optimal airfoil are evaluated in detail by full turbulence calculation (using SST turbulence model) based on Reynolds Averaged Navier-Stokes (RANS) equations, the size of O type grids for the evaluated airfoil is 298×140, and the far field is set to 60 times the chord length of the airfoil. The comparisons of design indicators between baseline and optimal airfoil with relative thickness of 26% are shown in Table 2. In the optimization of the airfoil with thickness of 26%, the drag coefficient of the optimized airfoil NWPU-CR-2601 is increased at the first design point, the drag reduction is achieved at other design points in the range of Mach 0.3 to Mach 0.5. Table 3 shows the constraint values of the optimal airfoil with relative thickness of 26%. It can be found that all the constraints are satisfied, the performance of pitching moment coefficient of the optimal airfoil NWPU-CR-2601 is ensured in a wide range of Mach numbers and angles of attack. The area and relative thickness of the optimal airfoil are not less than that of the baseline airfoil, which ensures the structural performance of the airfoil installed on the blades.

Table 2 – Comparisons of design indicators between baseline and optimal airfoil with relative thickness of 26%

Design points	Design Indicators	DBLN526	NWPU-CR-2601	Δ(%)
1.Ma=0.2, Re=1.4×10^6, α=±2°(reverse)	$\overline{C}_d^1$	0.02443203	0.02569686	+5.17694795
2.Ma=0.3, Re=2.2×10^6, α=±6°	$\overline{C}_d^2$	0.02545302	0.02403697	-5.56339819
3.Ma=0.4, Re=2.9×10^6, α=±4°	$\overline{C}_d^3$	0.02420315	0.02257095	-6.74375060
4.Ma=0.5, Re=3.6×10^6, α=±2°	$\overline{C}_d^4$	0.02431522	0.02248645	-7.52107881

Table 3 – Constraint values of optimal airfoils with relative thickness of 26%

Constraints	DBLN526	NWPU-CR-2601	Constraint Values
g_1	0.07851600	0.07396300	0.004553≤ 0.005
g_2	0.26067321	0.26603968	0.00536647≥ 0
g_3	0.20067655	0.20820642	0.00752987≥ 0

Similarly, from Table 4 and Table 5, it can be seen that the design indicators at all design points of the optimal airfoil NWPU-CR-4001 are improved with all constraints being satisfied, the drag coefficients are reduced in the range of Mach 0.3 to Mach 0.5, the pitching moment coefficient performance is maintained to a certain extent, and the area and relative thickness of the optimal airfoil are not less than that of the baseline airfoil.

Table 4 – Comparisons of design indicators between baseline and optimal airfoil with relative thickness of 40%

Design points	Design Indicators	NWPU-CR-4000	NWPU-CR-4001	Δ (%)
1.Ma=0.3, Re=2.2×10^6, α=±10°(reverse)	$\overline{C}_d^1$	0.05539229	0.05434355	-1.89328758
2.Ma=0.4, Re=2.9×10^6, α=±6°(reverse)	$\overline{C}_d^2$	0.04996423	0.04923111	-1.46730112
3.Ma=0.5, Re=3.6×10^6, α=±2°(reverse)	$\overline{C}_d^3$	0.05050312	0.05020537	-0.58955213
4.Ma=0.3, Re=2.2×10^6, α=±10°	$\overline{C}_d^4$	0.05537095	0.05427432	-1.98050906
5.Ma=0.4, Re=2.9×10^6, α=±6°	$\overline{C}_d^5$	0.04991898	0.04917273	-1.49490331
6.Ma=0.5, Re=3.6×10^6, α=±2°	$\overline{C}_d^6$	0.05045190	0.05016394	-0.57076242

Table 5 – Constraint values of optimal airfoils with relative thickness of 40%

Constraints	NWPU-CR-4000	NWPU-CR-4001	Constraint Values
g_1	0.11448250	0.11355350	0.000929≤ 0.005
g_2	0.40164000	0.40526000	0.003620≥ 0
g_3	0.30857000	0.30952000	0.000950≥ 0

3.2.2 Aerodynamic Performance Using Free Transition Calculation

To further explore the aerodynamic performance of the airfoils before and after optimization, in this sub-section, the baseline and the optimal airfoil are evaluated by free transition calculation (using γ-$Re_{\theta t}$ transition model) based on RANS equations. The laminar flow and airflow separation play important roles on the surface of large thickness airfoil, therefore, the transient simulation with transition model can bring more details and it is easier to understand the flow mechanism in airfoil optimization and design. The results show that there are vortex shedding and generation on the surface of leading edge of the airfoil in reverse flow (Figure 4, Figure 5), which lead to the oscillation of aerodynamic coefficient. Figure 3 shows the comparisons of the pulsation of lift coefficients between baseline and optimal airfoils. The last few time steps after the constant amplitude oscillation are selected to compare the vibration of airfoils before and after optimization. The results show that the pulsation of lift coefficient of the optimized airfoil is lower than that of the baseline airfoil in the

two airfoil optimization problems, which means that the vibration of the optimized airfoils can be alleviated to a certain extent in reverse flow.

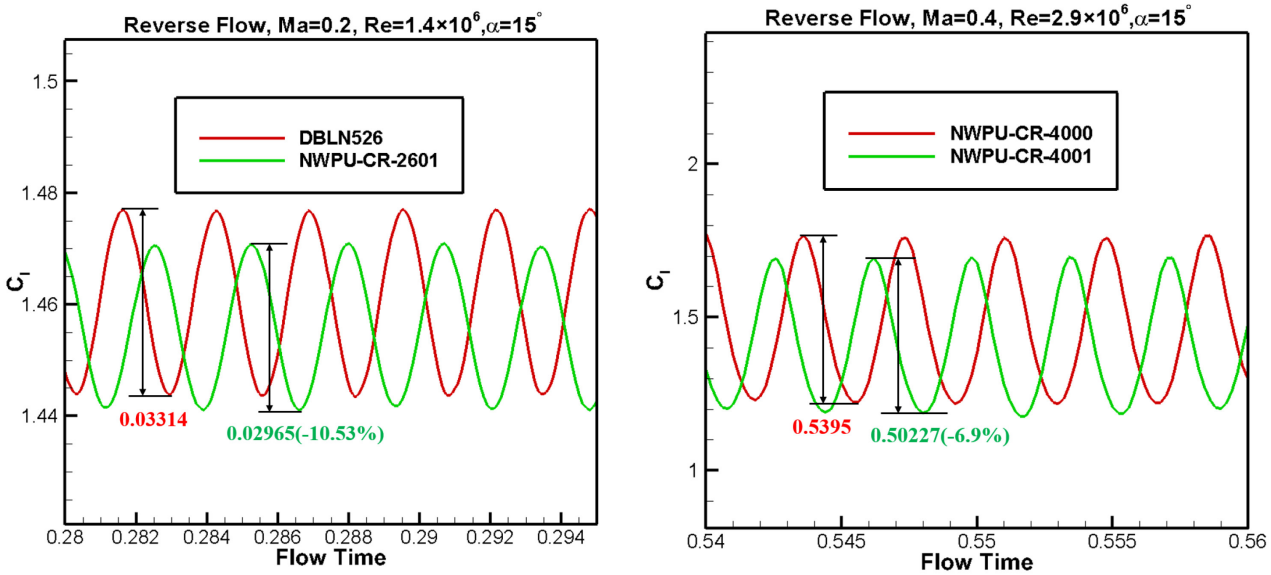

Figure 3 – Comparisons of the pulsation of lift coefficients between baseline and optimal airfoils.

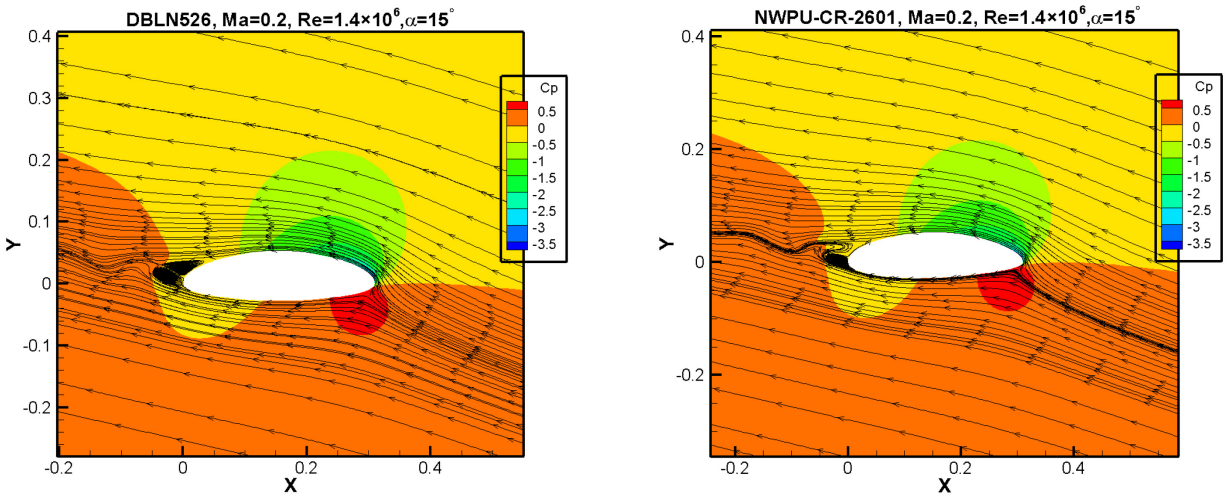

Figure 4 – Streamlines of baseline and optimal airfoil with relative thickness of 26%.

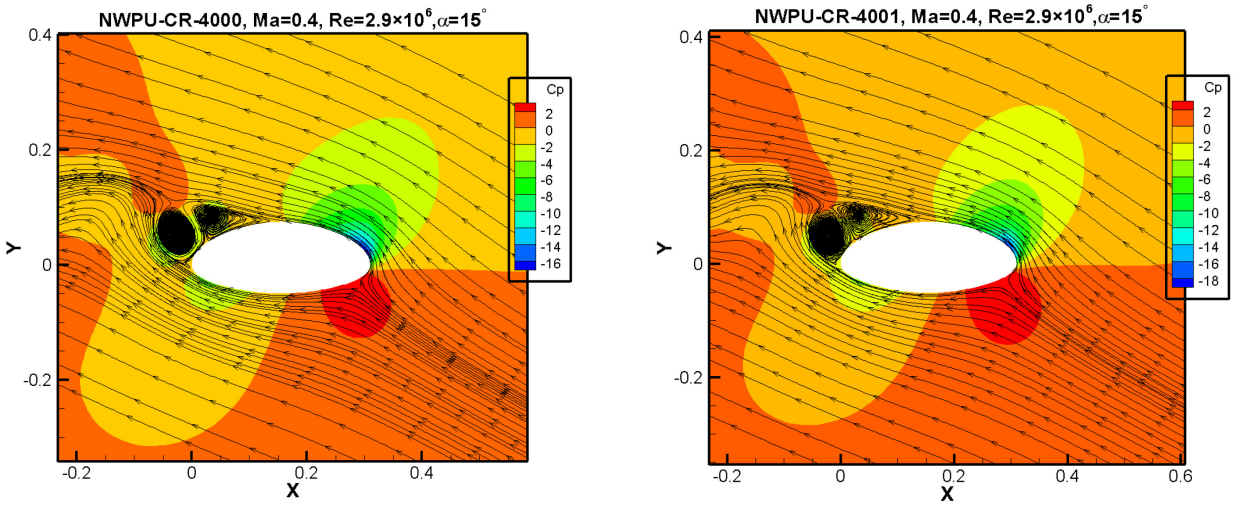

Figure 5 – Streamlines of baseline and optimal airfoil with relative thickness of 40%.

4. Conclusions

In this paper, a multi-objective aerodynamic optimization design method based on Kriging models is established, in the sub-optimization, an infill-sampling strategy based on hypervolume is used to find the optimum design. By analyzing the working environment and flow field of the large thickness airfoil at the root segment of the coaxial rigid rotor blades, the design points, optimization objectives and constraints are obtained. The purpose is to reduce the drag coefficient of double blunt rotor airfoils with relative thicknesses of 26% and 40% in forward flow and reverse flow in the working range of Mach numbers. After the optimization is completed, full turbulence calculation and free transition calculation based on RANS equations are performed on the airfoils before and after optimization. The results show that:

1) In the full turbulence calculation, the design indicators of the optimal airfoil with relative thickness of 26% in forward flow are all improved with all constraints being satisfied, and the drag coefficient at each design point in the wide range of Mach numbers is reduced. The drag coefficient in reverse flow at Mach 0.2 is improved, which requires further exploration of the weight coefficients and design space.

2) In the full turbulence calculation, the design indicators of the optimal airfoil with relative thickness of 40% are all improved with all constraints being satisfied in both forward and reverse flow, the drag coefficients are reduced in the range of Mach 0.3 to Mach 0.5.

3) In the free transition calculation with γ-$Re_{\theta t}$ transition model, there are vortex shedding and generation on the surface of leading edge of the airfoil in reverse flow, which lead to the oscillation of aerodynamic coefficient. The pulsation of lift coefficient of the optimized airfoil is lower than that of the baseline airfoil in the two airfoil optimization problems, which means that the vibration of the optimized airfoils can be alleviated to a certain extent in reverse flow.

5. Contact Author Email Address

ymyao@mail.nwpu.edu.cn

6. Copyright Statement

References

[1] Burgess Robert K. The ABC Rotor -A historical perspective[C]. Baltimore, *American Helicopter Society 60th Annual Forum*, 2004.

[2] Linden Arthur W. Fifty years of Sikorsky high speed concepts[C]. *American Helicopter Society 64th Annual Forum,* 2008.

[3] Bagai Ashish. Aerodynamic of the X2 technology demonstrator™ main rotor blade[C]. *Annual Forum of the American Helicopter Society,* 2008.

[4] Krige D G. A statistical approach to some basic mine valuation problems on the Witwatersrand. *Journal of the Chemical, Metallurgical and Mining Engineering Society of South Africa*, Vol. 52, No. 6, pp 119-139, 1951.

[5] Forrester A I J and Keane A J. Recent advance in surrogate-base optimization. *Progress in Aerospace Science,* Vol. 45, No. 1, pp 50-79, 2009.

[6] Wilson B, Cappelleri D, Simpson T W and Frecker M. Efficient Pareto frontier exploration using surrogate approximation. *Optimization and Engineering,* Vol. 2, No. 1, pp 31-50, 2001.

[7] Ahmed M and Qin N. Surrogate-based multi-objective aerothermodynamic design optimization of hypersonic spiked bodies. *AIAA Journal,* Vol. 50, pp 797-810, 2012.

[8] Sugimura K, Jeong S, Obayashi S and Kimura T. Kriging-model-based multi-objective robust optimization and trade-off-rule mining using association rule with aspiration vector. *Eleventh Conference on Congress on Evolutionary Computation,* 2009.

[9] Jones D R, Schonlau M and Welch W J. Efficient global optimization of expensive black-box functions. *Journal of Global Optimization* Vol. 13, pp 455-492, 1998.

[10] Kanazaki M, Tanaka K, Jeong S and Yamamoto K. Multi-objective aerodynamic exploration of elements' setting for high-lift airfoil using Kriging model. *Journal of Aircraft*, Vol. 44, No. 3, pp 858-864, 2007.

[11] Obayashi S. Multi-objective design exploration using efficient global optimization. *Proceedings of the European Conference on Computational Fluid Dynamics (ECCOMAS CFD),* TU Delft, pp 1-8, 2006.

[12] Zitzler E and Thiele L. Multiobjective evolutionary algorithms: A comparative case study and the strength Pareto approach. *IEEE Transactions on Evolutionary Computation*, Vol. 3, No. 4, pp 257-271, 1999.

[13] Beume N, Naujoks B and Emmerich M. SMS-EMOA: Multiobjective selection based on dominated hypervolume. *European Journal of Operational Research,* Vol. 181, No. 3, pp 1653-1669, 2007.

[14] Emmerich M, Deutz A H and Klinkenberg J W. Hypervolume-based expected improvement: Monotonicity properties and exact computation. *Evolutionary Computation (CEC), 2011 IEEE Congress on IEEE*, New Orleans, LA, USA, pp 2147-2154, 2011.

[15] Shimoyama K, Jeong S and Obayashi S. Kriging-surrogate-based optimization considering expected hypervolume improvement in non-constrained many-objective test problems. *IEEE Congress on Evolutionary Computation IEEE,* pp 658-665, 2013.

[16] Martínez-Frutos J and Herrero-Pérez D. Kriging-based infill sampling criterion for constraint handling in multi-objective optimization. *Journal of Global Optimization*, Vol. 64, No. 1, pp 97-115, 2016.

[17] Zuhal L R, Amalinadhi C, Dwianto Y B, Palar P S and Shimoyama K. Benchmarking multi-objective Bayesian global optimization strategies for aerodynamic design, *2018 AIAA/ASCE/AHS/ASC Structures, Structural Dynamics, and Materials Conference*, 2018.

[18] Knowles J. ParEGO: a hybrid algorithm with on-line landscape approximation for expensive multiobjective optimization problems. *IEEE Transactions on Evolutionary Computation*, Vol. 10, No. 1, pp 50-66, 2006.

[19] HAN Z H, XU C Z, QIAO J L, et al. Recent progress of efficient global aerodynamic shape optimization using surrogate-based approach. *Acta Aeronautica et Astronautica Sinica,* Vol. 41, No. 3, pp 30-70 (in Chinese), 2020.

[20] Kulfan B M and Bussoletti J E. Fundamental parametric geometry representations for aircraft component shapes. *11th AIAA/ISSMO Multidisciplinary Analysis and Optimization Conference*, 2006.

[21] Drela M. XFOIL: An analysis and design system for low Reynolds number airfoils. *Conference on Low Reynolds Number Airfoil Aerodynamics*, University of Notre Dame, 1989.